Excitation of low-*n* toroidicity induced Alfvén eigenmodes by energetic particles in global gyrokinetic tokamak plasmas

Y. Nishimura[a)]

Plasma and Space Science Center, National Cheng Kung University, Tainan 70101, Taiwan

The first linear global electromagnetic gyrokinetic particle simulation on the excitation of toroidicity induced Alfvén eigenmode (TAE) by energetic particles is reported. It is shown that the long wavelength magnetohydrodynamic instabilities can be studied by the gyrokinetic particle simulation. With an increase in the energetic particle pressure, the TAE frequency moves down into the lower continuum together with an increase in the linear growth rate. © *2009 American Institute of Physics*. [DOI: 10.1063/1.3088028]

Toroidicity induced Alfvén eigenmode[1–3] (TAE) can play important roles in burning plasmas. The TAE modes can be excited when energetic particles, for example, fusion born alpha particles, resonate with the phase velocity of the shear Alfvén wave which resides within the frequency gap of the Alfvén continuum.

Shear Alfvén wave oscillations, continuum damping, and the appearance of the frequency gap in toroidal geometries by gyrokinetic particle simulation have been recently reported.[4] The simulation of Ref. 4 is demonstrated in the long wavelength magnetohydrodynamic (MHD) like limit in the absence of kinetic ions. In this letter, taking exactly the same parameters[3,4] but adding the energetic ion particles, the first linear particle simulation on the excitation of the TAE modes is reported. The simulation is done without employing MHD equation. The simulation is not the conventional gyrokinetic-MHD hybrid ones,[5–10] where the kinetic ions enter the system through the stress tensor. The setting of the simulation is kept as faithful as possible to Refs. 3 and 4 to see an explicit connection with our previous studies.[4]

A simplified linearized set of equations is employed[11] for the numerical simulation which is reduced from the electron-fluid ion-kinetic hybrid gyrokinetic model.[12–15] The equations of Ref. 4 are normalized by the ion Larmor radius (at the electron temperature) for the length, the ion cyclotron frequency for time, and the electron temperature for the electrostatic potential, and the magnetic field strength at the magnetic axis, B_0. The set of the equations are the electron continuity equation

$$\frac{\partial \delta n_e}{\partial t} = -\nabla_\parallel \delta u_{\parallel e} \qquad (1)$$

(δn_e is the fluid electron density and $\delta u_{\parallel e}$ is parallel electron velocity), the inverse of Faraday's law

$$\frac{\partial A_\parallel}{\partial t} = \nabla_\parallel (\Phi_{\text{eff}} - \Phi) \qquad (2)$$

($A_\parallel$ is the vector potential, Φ is the electrostatic potential, and Φ_{eff} is the effective potential representing the total parallel

electric field), the gyrokinetic Poisson equation[16]

$$\Phi - \tilde{\Phi} = \delta\overline{n}_\alpha - \delta n_e \qquad (3)$$

($\delta\overline{n}_\alpha$ is the gyroaveraged energetic particle density, $\tilde{\Phi}$ is the second gyrophase averaged electrostatic potential[16]), the lowest order adiabatic relation

$$\Phi_{\text{eff}} = \delta n_e, \qquad (4)$$

and the inverse of Ampere's law

$$\delta u_{\parallel e} = \beta_e^{-1}\nabla_\perp^2 A_\parallel + \delta u_{\parallel \alpha}. \qquad (5)$$

The parallel velocity of the energetic particles is given by $\delta u_{\parallel \alpha}$. Here $\beta_e = (c_s/v_A)^2$ where c_s is the sound velocity and v_A is the Alfvén velocity. As we can see in Eq. (2), we impose $\partial_t A_\parallel$ to be in a potential form $\nabla_\parallel(\Phi_{\text{eff}} - \Phi)$. In other words, the $k_\parallel = 0$ component of the inductive parallel electric field is removed (here, $k_\parallel$ is the wave vector parallel to the equilibrium magnetic field) and thus the dynamics related to the collisionless magnetic reconnection are discarded in the current model. All the variables in Eqs. (1)–(5) are the normalized ones. The gradient operators $\nabla_\perp$ and $\nabla_\parallel$ are those in the direction perpendicular and parallel to the equilibrium magnetic field.

By coupling Eqs. (1)–(5), the shear Alfvén wave dispersion relation in the toroidal geometry, Eq. (2) of Ref. 3 can be obtained. Figure 1 shows the shear Alfvén wave frequency as a function of the radial coordinate r (a is the minor radius), which is equivalent to Fig. 1 of Ref. 3. Due to the $1/R$ variation of the toroidal magnetic field (R is the major radius), the cylindrical Alfvén continuum (dashed lines) breaks up and the frequency gap (or the frequency forbidden band) appears within the range of $0.299 < \omega/\omega_A < 0.389$. Here, $\omega_A = v_A/q_0 R_0$ is the Alfvén frequency at the magnetic axis (q_0 is the safety factor and R_0 is the major radius at the magnetic axis, respectively).

Equations (1)–(5) are employed (with the $\delta\overline{n}_\alpha$ and $\delta u_{\parallel \alpha}$ terms *turned off*) in the simulation of Fig. 5 of Ref. 4. On top of Eqs. (1)–(5) we add kinetic ions. The guiding center equation and the δf gyrokinetic equation (the weight equation) (Ref. 17) are solved for the kinetic energetic particle ions (we neglect thermal kinetic ions, however). Taking the per-
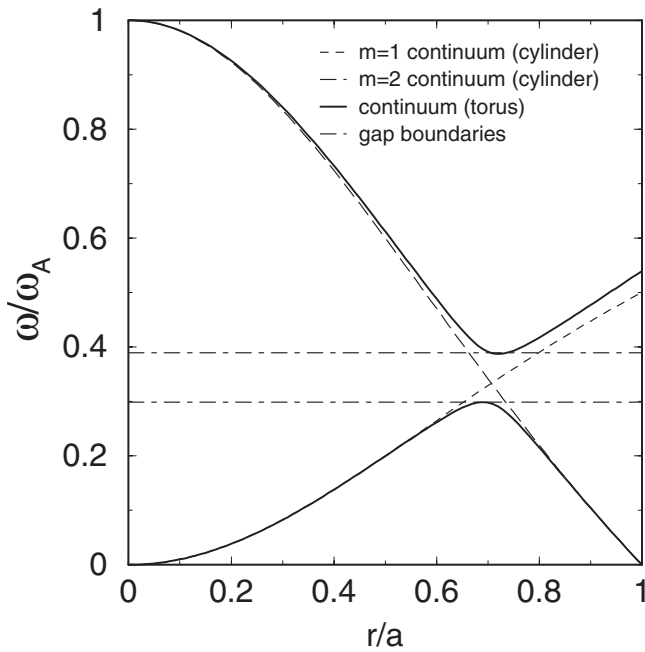
FIG. 1. Shear Alfvén frequency as a function of the radial location. The dashed curves are the continuum frequencies for the cylindrical limit, for $m=1$ and $m=2$ modes. The solid lines are for the continuum frequency with the toroidal geometry effect. The lower (upper) boundary of the upper (lower) curve is at $\omega/\omega_A=0.389$ ($\omega/\omega_A=0.299$). Correspondingly the frequency gap (the forbidden frequency range) appears within the range of $0.299 < \omega/\omega_A < 0.389$. The figure is produced by employing Eq. (8) of Ref. 3, which corresponds to Fig. 1 of Ref. 3.

turbed distribution function δf_α, the energetic particle density in Eq. (3) is given by

$$\delta \overline{n}_\alpha = r_\alpha \int \delta f_\alpha d^3 v \qquad (6)$$

and the parallel velocity of the energetic particles in Eq. (5) is given by

$$\delta u_{\|\alpha} = r_\alpha \int v_\| \delta f_\alpha d^3 v, \qquad (7)$$

where $\int d^3 v$ is an average over the velocity space. Note that in the simulation, we control the perturbed density of the energetic particles by multiplying a factor r_α ($r_\alpha < 1$) which is proportional to the equilibrium energetic particle density. As we discuss below, r_α is proportional to the pressure (the beta value) of the energetic particles. The energetic ion particles are provided with the Maxwellian distribution function $f_{0\alpha} \propto \exp\left(-v_\|^2/2v_\alpha^2\right)$ in the velocity space (thus $\partial f_{0\alpha}/\partial v_\|$ is always negative).[18] The thermal velocity of the Maxwellian distribution function is of the order of Alfvén speed, and thus there exist finite numbers of resonating energetic particles within the frequency gap.

The particles that resonate with the shear Alfvén wave with the phase velocity $\omega/k_\|$ can destabilize the TAE mode, when the mode frequency ω is within the frequency gap (we choose $\omega/\omega_A=0.344$ in the middle of the gap in Fig. 1), and when the parallel wave vector $k_\| = (m - nq)/qR$ satisfies $k_\| = -k_{\|m} = k_{\|m+1}$ at $q = (2m+1)/2n$. Here, m (n) stands for the poloidal (toroidal) mode number. We take $m=1$, $m+1=2$,

and $n=1$ which is equivalent to $m=-2$, $m+1=-1$, and $n=-1$ of Ref. 3. The geometrical parameters used for the simulation are the same as in Refs. 3 and 4 (for example, the inverse aspect ratio of 0.375 and a parabolic safety factor q). The major radius is given by $R=46.6$ cm as well (after convincing the TAE excitation in the originally published setting,[4] we move on to a parameter survey in a larger size plasma). From the ω and the $k_\|$ values chosen above, we provide the Maxwellian distribution with $v_\alpha = \omega/k_\| = 10.32c_s$. The mass and the charge of the energetic particles are that of the hydrogen ion. In the specific simulation below, we set $\beta_e = 0.01$, and the constant density gradient $\kappa_n = -R(1/n_\alpha) \times (dn_\alpha/dr) = 8.0$. Here, n_α represents the equilibrium density of the energetic particles. The temperature gradient parameters[4] are set to be zero. In Eqs. (6) and (7), $r_\alpha = 0.15$ is taken for Figs. 2 and 3.

The simulation is conducted by an electromagnetic extension[4] of the GTC code[19–21] with a noniterative field solver.[22,23] With the additional energetic particle drive, the TAE mode is excited. A linear eigenmode (contour plot) of the TAE instability is shown in Fig. 2. Note that the contour plots are not up-down symmetric.[24]

The frequency spectrum of the TAE instability is shown in Fig. 3. The global mode frequency ($\omega/\omega_A = -0.36$) found within the gap (and not on the gap boundaries as in Ref. 4)[25] is a clear evidence of the TAE excitation. The linear growth rate of the TAE instability is given by $\gamma/\omega_A = 0.0215$ (and thus $|\gamma/\omega| = 6.0\%$) for both the $m=1$ and $m=2$ mode.

Figure 4 shows the linear TAE growth rates (divided by the real frequency) versus the multiplication factor r_α. Compared to the calculations in Figs. 2 and 3, a twice larger plasma size is taken for Fig. 4 (the Larmor radius of the energetic particles in Figs. 2 and 3 is 15% of the minor radius while 7.5% in Fig. 4). We see a monotonic increase in the growth rate as the energetic particle population increase (and thus the effective beta value of the energetic particles, β_α increases; at $\beta_e = 0.01$, a simple estimate will give $\beta_\alpha = 4\pi n_\alpha T_\alpha / B_0^2 \sim r_\alpha$. Here T_α is the energetic particle temperature). On the other hand, the real frequency of the mode decreases (approximately 15% of a reduction in the real frequency) as r_α (or β_α) increases and crosses the lower gap boundary[26] (but not the upper gap boundary) which is suggested by the analysis in Ref. 27. (Resonant TAE, which emphasizes the resonance between the mode frequency and the magnetic drift frequency of the energetic particles.)[27] As a reference, the energetic particle mode (EPM)[28] refers to the heating of the continuum based on the notion that the energetic particle drive exceeds the continuum damping and predicts the appearance of the mode frequency both in the upper and the lower continuum. The square plots in Fig. 4 represent the analysis of the TAE growth rate in a large aspect ratio tokamak from Ref. 3 (the simulation results and the analysis compare favorably at higher β_α. It will be interesting to further investigate the regime where the magnitudes of the linear growth rate and the real frequency become comparable[9]).

We note that instability growth was already minimal at $r_\alpha = 0.025$ (with the specific simulation parameters we employed in Fig. 4), and we did not survey below $r_\alpha < 0.025$ in
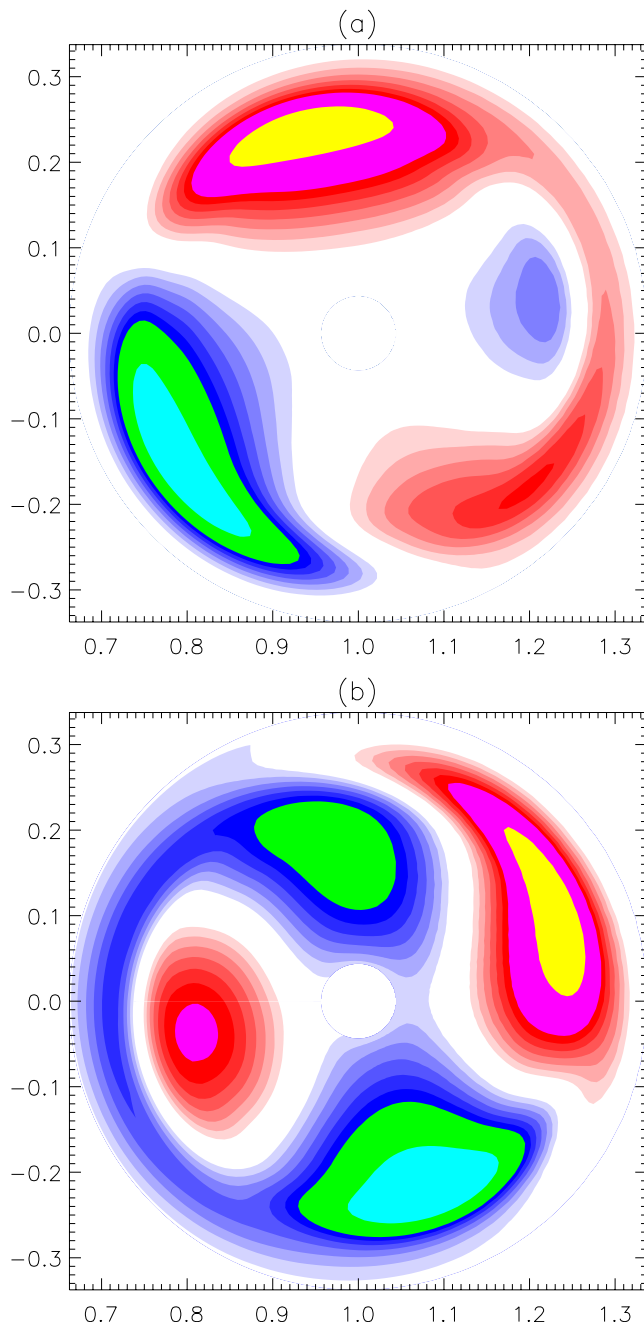
FIG. 2. (Color online) Linear eigenmodes (contour plots on a poloidal plane) of TAE instability. (a) The electrostatic potential Φ at a toroidal angle $\zeta=0$. (b) The vector potential $A_\parallel$ at a toroidal angle $\zeta=0$.

this work. The TAE mode in its nature should not have an instability threshold. The latter onset feature needs to be investigated in detail to see the limitation of the initial value approach (if any). In Fig. 4, eight energetic particles per cell are taken in the simulation. We plan to pursue the simulation with much larger numbers of particles. We also would like to remind that a simplified model Eqs. (1)–(5) is employed in this letter (so as to primary focus on the excitation of TAE by the additional energetic particles).[4] The radial extension of the simulation domain is limited to $0.1<r/a<0.9$ (see Fig. 2). An inclusion of the magnetic axis can be crucial to describe the long wavelength global modes precisely.
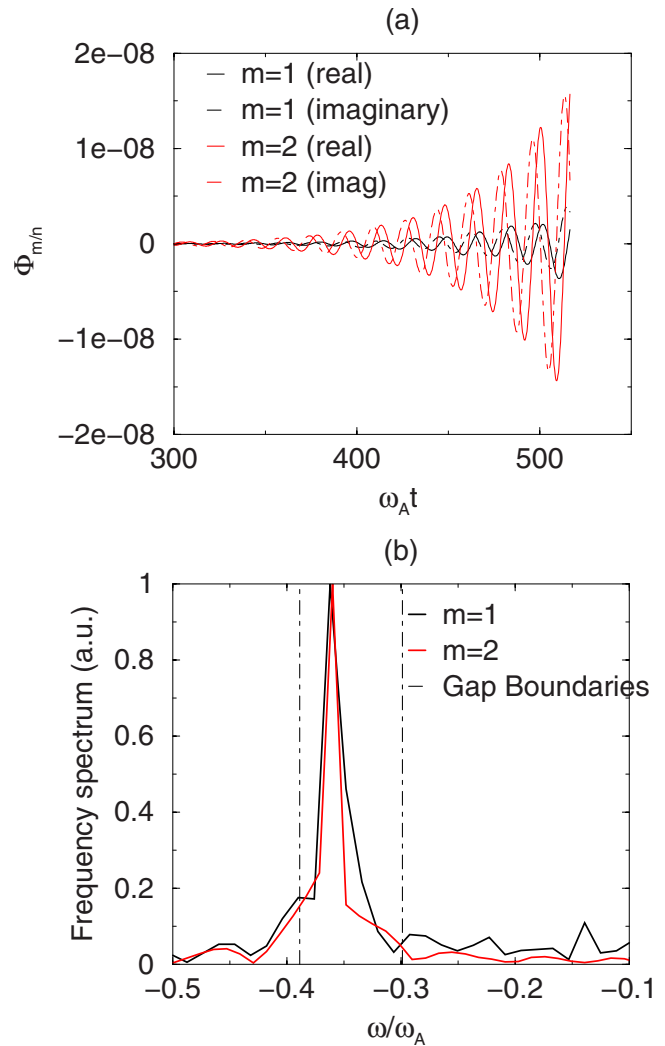
FIG. 3. (Color online) (a) The Fourier components of the electrostatic potential Φ as a function of time. (b) The frequency spectrum obtained from the time series of Fig. 3(a).
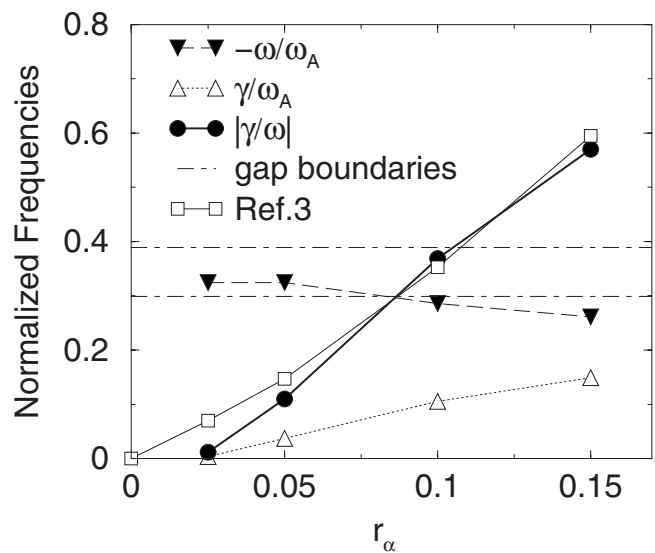
FIG. 4. Dependence of the real frequency ω, and the linear growth rate γ on r_α (and thus β_α). For each data, eigenmode structures similar to Fig. 2 are obtained. The squares represent the analytical TAE growth rate–real frequency ratio in a large aspect ratio tokamak from Ref. 3. The frequency gap boundaries are signified by the long dashed lines.

In summary, the first linear excitation of the low-n TAE modes by the energetic particles in a global gyrokinetic particle simulation is reported.[29] The work did not employ MHD model (through closure relations). With a completion of the current global gyrokinetic simulation method, one can investigate the onset and the saturation mechanism of the TAE modes simultaneously without any restrictions on the wavelength of the modes. Apparently, the advantage of initial value approach is its application for nonlinear simulation. We plan to report the analysis of energetic particles driven high-n Alfvénic modes separately. Whether which mode numbers are most unstable is a great interest to large tokamak burning plasma experiments.

[1] C. Z. Cheng, L. Chen, and M. S. Chance, Ann. Phys. (N.Y.) **161**, 21 (1985).

[2] C. Z. Cheng and M. S. Chance, Phys. Fluids **29**, 3695 (1986).

[3] G. Y. Fu and J. W. Van Dam, Phys. Fluids B **1**, 1949 (1989).

[4] Y. Nishimura, Z. Lin, and W. X. Wang, Phys. Plasmas **14**, 042503 (2007).

[5] W. Park, S. Parker, H. Biglari, M. Chance, L. Chen, C. Z. Cheng, T. S. Hahm, W. W. Lee, R. Kulsrud, D. Monticello, L. Sugiyama, and R. White, Phys. Fluids B **4**, 2033 (1992).

[6] G. Y. Fu and W. Park, Phys. Rev. Lett. **74**, 1594 (1995).

[7] C. Z. Cheng, J. Geophys. Res. **96**, 21159, DOI: 10.1029/91JA01981 (1991).

[8] S. Briguglio, G. Vlad, F. Zonca, and C. Kar, Phys. Plasmas **2**, 3711 (1995).

[9] S. Briguglio, F. Zonca, and G. Vlad, Phys. Plasmas **5**, 3287 (1998).

[10] Y. Todo and T. Sato, Phys. Plasmas **5**, 1321 (1998).

[11] These simplified equations are employed for the simulation of the Alfvén eigenmodes in Ref. 4 (but not for the microinstability part).

[12] Y. Chen and S. Parker, Phys. Plasmas **8**, 441 (2001).

[13] Z. Lin and L. Chen, Phys. Plasmas **8**, 1447 (2001).

[14] W. X. Wang, L. Chen, and Z. Lin, Bull. Am. Phys. Soc. **46**, 114 (2001).

[15] F. L. Hinton, M. N. Rosenbluth, and R. E. Waltz, Phys. Plasmas **10**, 168 (2003).

[16] W. W. Lee, J. Comput. Phys. **72**, 243 (1987).

[17] A. M. Dimits and W. W. Lee, J. Comput. Phys. **107**, 309 (1993).

[18] M. N. Rosenbluth and P. H. Rutherford, Phys. Rev. Lett. **34**, 1428 (1975).

[19] Z. Lin and W. W. Lee, Phys. Rev. E **52**, 5646 (1995).

[20] R. B. White and M. S. Chance, Phys. Fluids **27**, 2455 (1984).

[21] Z. Lin, T. S. Hahm, W. W. Lee, W. M. Tang, and R. B. White, Science **281**, 1835 (1998).

[22] Y. Nishimura, Z. Lin, J. L. V. Lewandowski, and S. Ethier, J. Comput. Phys. **214**, 657 (2006).

[23] Y. Nishimura and Z. Lin, Contrib. Plasma Phys. **46**, 551 (2006).

[24] J. Y. Kim, Y. Kishimoto, M. Wakatani, and T. Tajima, Phys. Plasmas **3**, 3689 (1996).

[25] We remind that the upper branch of the continuum accumulates more prominently than the lower branch as predicted at the zero resistivity limit of the periodic shear Alfvén wave mode (Refs. 1 and 27). See Fig. 5(b) of Ref. 4.

[26] N. N. Gorelenkov, C. Z. Cheng, and W. M. Tang, Phys. Plasmas **5**, 3389 (1998).

[27] C. Z. Cheng, N. N. Gorelenkov, and C. T. Hsu, Nucl. Fusion **35**, 1639 (1995).

[28] F. Zonca and L. Chen, Phys. Plasmas **3**, 323 (1996); L. Chen, *ibid.* **1**, 1519 (1994); L. Chen and F. Zonca, Phys. Scr. **T60**, 81 (1995).

[29] The TAE eigenmode structures by gyrokinetic particle simulation in the absence of energetic particles are exhibited in a very recent work by A. Mishchenko, R. Hatzky, and A. Könies, Phys. Plasmas **15**, 112106 (2008).